

Signal model for the reconstruction of inclined air showers with sparse radio arrays

Felix Schlüter^{a,b,*} and Tim Huege^{a,c}

^aKarlsruher Institut für Technologie, Institut für Astroteilchenphysik, Karlsruhe, Germany

^bUniversidad Nacional de San Martín, Instituto de Tecnologías en Detección y Astropartículas, Buenos Aires, Argentina

^cVrije Universiteit Brussel, Astrophysical Institute, Brussels, Belgium

E-mail: fschluter@icecube.wisc.edu, tim.huege@kit.edu

We present a signal- and reconstruction model for the radio emission of extensive air showers with zenith angles between 65° and 85° in the 30-80 MHz band. The model is derived from CoREAS simulations and explicitly takes into account the asymmetries introduced by the superposition of charge-excess and geomagnetic radiation as well as by early-late effects. We exploit correlations among fit parameters to reduce the dimensionality, thereby ensuring stability of the fit procedure. Our approach reaches a reconstruction efficiency near 100% with an intrinsic resolution for the reconstruction of the electromagnetic energy below 5% using a 1.5 km-sparse antenna array. It can be employed in upcoming large-scale radio detection arrays using the 30-80 MHz band, in particular the Auger Radio detector of the upgraded Pierre Auger Observatory, and can likely be adapted to experiments such as GRAND operating at higher frequencies.

Acoustic & Radio EeV Neutrino Detection Activities (ARENA)

7–10 Jun 2022

Santiago de Compostela, Spain

*Speaker

Table 1: CORSIKA simulation settings for the two different simulation sets.

	Development	Validation
Release	v7.69 ¹	v7.7
Number of showers	4309	15970
Primaries	p, Fe	p, He, N, Fe
Energies E / eV	$10^{18.4}, 10^{18.6}, \dots, 10^{20.2}$	$[10^{18.4}, 10^{20.1}]$ flat in \log_{10}
Zenith angles θ	$65^\circ, 67.5^\circ, \dots, 85^\circ$	$[65^\circ, 85^\circ]$ flat in \sin^2
Azimuth angles ϕ	$0^\circ, 45^\circ, \dots, 315^\circ$	$[0^\circ, 360^\circ)$
h.e. had. int. model	QGSJETII-04 [8]	QGSJETII-04, Sibyll2.3d [9, 10]
l.e. had. int. model	UrQMD [11]	UrQMD
Thinning ϵ_{thin}	5×10^{-6}	1×10^{-6}
STEPFC		1 (default)

1. Introduction

Radio detection of inclined air showers is appealing for two reasons: First, inclined air showers illuminate large footprints at ground which enables their detection with kilometer-spaced antenna arrays. Such sparse arrays can be scaled up in size to provide sufficient aperture to detect cosmic rays at the highest energies $\sim 10^{20}$ eV. And second, radio antennas are sensitive to only the electromagnetic shower component while particle detectors solely measure muons from inclined air showers. Combining those complementary measurements yields a large sensitivity to the mass composition of ultra-high-energy cosmic rays [1–4].

While the Pierre Auger Observatory has already demonstrated the detection of inclined air showers with kilometer-spaced radio antennas of its Auger Engineering Radio Array [5, 6], and with the 3000 km² Radio Detector of the upgrade Pierre Auger Observatory routinely detecting those events in the near future, we lack a dedicated signal model to describe the measured emission pattern and reconstruct the air shower energy. Here, we present a signal model for the description of the highly asymmetric lateral radio-signal distribution from inclined air showers with zenith angles above 65° – the “radio-emission footprints”. We use a comprehensive set of CoREAS simulations to exploit correlations between the model parameters and air shower observables allowing us to describe all radio-emission footprints with only two parameters: the geomagnetic radiation energy E_{geo} and the distance between the shower maximum and the shower impact point at the ground d_{max} . The derived parameterizations are suited for the Pierre Auger Observatory, the adaptation of the model to other experiments is discussed in the end. All detail regarding the model can be found in [7].

2. Simulations of inclined air showers

We use the simulation codes CORSIKA [12] and CoREAS [13] to generate the particle cascades and radio emission, respectively. We classify our simulations in two sets which mainly differ in their

¹This version was modified with an optimization for inclined air showers which was published with v7.7.

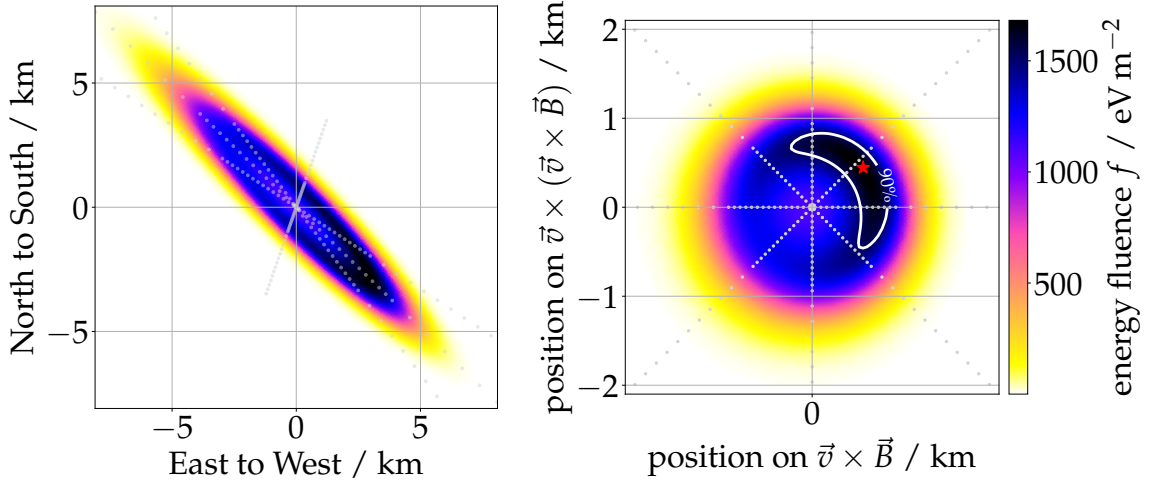


Figure 1: The simulated radio emission of an 80° CoREAS shower displayed in the ground plane (*left*) and in the shower plane (*right*). The radio-emission is simulated at 240 positions (shown as gray dots) and interpolated in between. The color code shows the (total) energy fluence, i.e., the energy deposit per unit area in the 30 MHz to 80 MHz band. See detail in text.

detector layout and purpose: To develop our signal model, we use simulations with an unrealistically dense detector layout which allows a high fidelity sampling of the showers' footprints. To evaluate the performance of our model, we use simulations with a more realistic, 1.5 km sparse detector layout. For both sets, the simulated ambient condition match those present at the Pierre Auger Observatory in October. Other simulation settings are summarized in table 1.

3. Radio emission from inclined extensive air showers

Inclined air showers induce large, highly elongated, complex radio-emission footprints at ground. Fig. 1 (*left*) shows the emission pattern of a 80° inclined CoREAS shower arriving from South-East illuminating an area of several square kilometers. The footprint in terms of the energy fluence f , i.e., the energy deposit per unit area, exhibits significant asymmetries. For a better description of these asymmetries and to remove the elongation due to projection, we describe the footprint in a specific shower plane coordinate system perpendicular to the shower incoming direction as shown in Fig. 1 (*right*). The x - and y -axes are rotated such that they align with the $\vec{v} \times \vec{B}$ - and $\vec{v} \times (\vec{v} \times \vec{B})$ - directions, respectively. Here, \vec{v} is the shower direction (movement of particles) and \vec{B} is the direction of the Earth magnetic field. This allows an easier interpretation/description of the asymmetries via the superposition of the geomagnetic emission which is polarized in $\vec{v} \times \vec{B}$ -direction and charge-excess emission which is radially inwards polarized [14–16]. However, other than expected from the superposition of the two emission mechanisms, we find the maximum of the emission pattern not along the positive $\vec{v} \times \vec{B}$ axis but rotated counter-clockwise. This rotation is caused by an additional asymmetry which is mostly affecting inclined air showers. Due to the large elongation of the radio-emission footprint, observers in the incoming direction of the air shower are considerably closer to the origin of the radio emission than observers on the other side of the footprint. This has two effects: First, observers in the direction of the shower measure the radio

emission at an “earlier” and observers at the opposite side at a “later” stage of expansion, hence the intensity of the emission and thus the electric field amplitude is larger for early observers and smaller for late observers. And second, the axis distance r , i.e., the distance between observer and shower axis, of early observer is smaller than for a late observer, although they see the shower origin at the same off-axis angle. Both effects cause the so-called early-late asymmetry. When correcting for those two effects, the well-known interference pattern between the geomagnetic and charge-excess emission reemerges as we will see later. On top of those asymmetries a ring-like feature is visible which stems from a Cherenkov-like temporal compression of the radio emission [17]. At a particular lateral distance, the emission from the entire cascade arrives almost simultaneously creating a very strong coherent signal. Hence, this feature is typically called Cherenkov ring and the radius r_0 of the ring can be approximated with

$$r_0 = \tan(\delta_{\text{Che}}) d_{\text{max}} \quad \text{with} \quad \delta_{\text{Che}} = \cos^{-1}(1/n(h = h_{\text{max}})), \quad (1)$$

where $\delta_{\text{Che}}(h = h_{\text{max}})$ is the Cherenkov angle for a point source moving with the speed of light ($\beta = 1$) and $n(h_{\text{max}})$ is the refractive index at the shower maximum at an altitude h_{max} .

As already known from vertical showers, the strength of the geomagnetic emission increases with decreasing air density at the shower maximum. This trend continues for inclined air showers and manifests the geomagnetic emission as the clearly dominant mechanism over the charge-excess emission. In the context of this work (see [7]) and in [18], it was found that the charge-excess emission decreases in strength with decreasing air density which further reduces the contribution of the charge-excess emission at the highest inclinations. While in the lower half of the here considered zenith angle range, the interference of the both emission mechanisms has the largest contribution to the observed asymmetry, in the upper half, the early-late asymmetry is dominant. We also consider the refractive displacement of the radio-emission footprint from the shower axis described in [19].

4. Signal model

The signal model relies on three pillars: I) the correction of the aforementioned early-late asymmetry, II) a description of the lateral signal distribution of the geomagnetic emission with a rotationally symmetric lateral distribution function (LDF), and III) a parameterization of the charge-excess fraction to describe the asymmetry introduced by the superposition of the two emission mechanisms. For II) and III), we have to disentangle the emissions from both mechanisms. Following the approach in [20] we derive:

$$f_{\text{geo}} = \left(\sqrt{f_{\vec{v} \times \vec{B}}} - \frac{\cos \phi}{|\sin \phi|} \cdot \sqrt{f_{\vec{v} \times (\vec{v} \times \vec{B})}} \right)^2, \quad f_{\text{ce}} = \frac{1}{\sin^2 \phi} \cdot f_{\vec{v} \times (\vec{v} \times \vec{B})}, \quad (2)$$

with ϕ the polar angle of an observer w.r.t. the positive $\vec{v} \times \vec{B}$ axis. Note that Eqs. (2) applied on data would allow us to describe the radio-emission footprint without the need to parameterize a charge-excess fraction. However, using a parameterization of the charge-excess fraction, we can base the description of the entire footprint on the signal measured in the $\vec{v} \times \vec{B}$ polarization only, which, due to the particular polarization pattern, has a higher signal-to-noise ratio than a measurement of the signal in the $\vec{v} \times (\vec{v} \times \vec{B})$ polarization, in particular for inclined air showers.

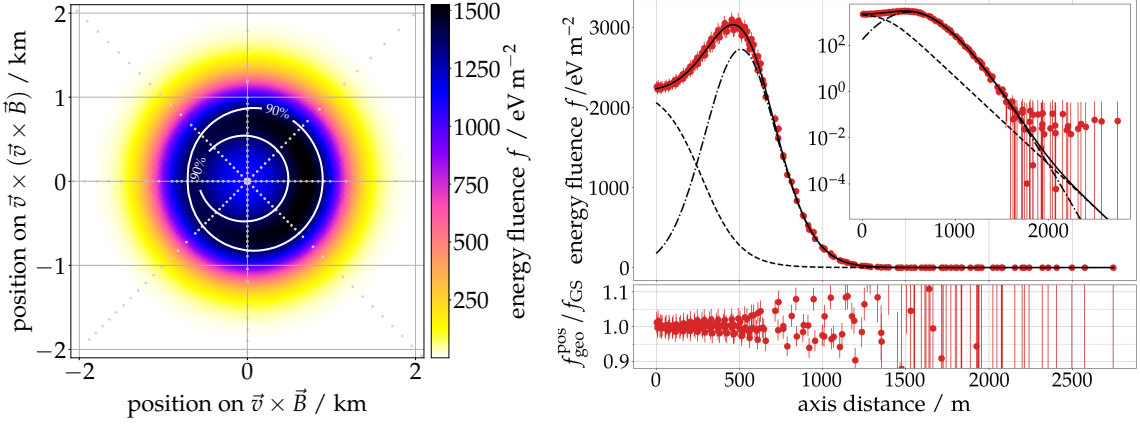


Figure 2: *Left:* Early-late corrected radio-emission footprint of the same shower as in Fig. 1. *Right:* Lateral distribution of the geomagnetic emission in terms of its energy fluence (red markers). The distribution is accurately described by the LDF $f_{GS}(r)$ which is the sum (solid line) of a Gaussian (dashed-dotted line) and a sigmoid (dashed line). The bottom panel shows the relative deviation between $f_{GS}(r)$ and the true signal distribution $f_{geo}^{pos}(r)$ according to Eq. (2). The tail of the lateral distribution exhibits a nonphysical flattening due to thinning which is compensated for by setting appropriate uncertainties. The inset shows the same data with a logarithmic scaling along the y-axis.

To correct for the early-late effects, i.e., remove the asymmetry, we assume that the radio emission originates from a point source located on the shower axis at the shower maximum. This allows us to construct a purely geometrical correction based on the distance of the shower maximum d_{max} and that of an observer $z_i = \vec{x}_i \cdot \vec{e}_v$ to the shower plane at the ground, respectively. With a correction factor c_{el} , we correct energy fluence and axis distance as follows

$$f = f_{raw} \cdot c_{el}^2, \quad r = r_{raw} / c_{el}, \quad \text{with} \quad c_{el} \equiv \frac{d_{max} + \vec{x}_i \cdot \vec{e}_v}{d_{max}} = 1 + \frac{z_i}{d_{max}}, \quad (3)$$

where the unit vector \vec{e}_v points into the direction of the primary particle trajectory and “raw” donates the uncorrected quantities. This correction effectively projects all observers on one common plane perpendicular to the shower direction. In Fig. 2 (*left*) the early-late corrected radio-emission footprint of the shower shown in Fig. 1 is shown. With the correction applied, the asymmetry is considerably reduced. Furthermore, the remaining asymmetry is consistent with the expected interference pattern of the two emission mechanisms. A more quantitative evaluation yields a resolution of better than 5% for all observers within 2.5 Cherenkov radii around the shower axis, see [7] for more details.

With the above correction, the signal distribution of the pure geomagnetic emission is rotationally symmetric and can be described by a 1-dimensional LDF, as shown in Fig. 2 (*right*). The signal distribution is described with the following formula:

$$f_{GS}(r) = f_0 \left[\exp \left(- \left(\frac{r - r_0^{fit}}{\sigma} \right)^{p(r)} \right) + \frac{a_{rel}}{1 + \exp \left(s \cdot [r / r_0^{fit} - r_{02}] \right)} \right]. \quad (4)$$

which is the sum of a Gaussian and sigmoid with seven free parameters. For the six parameters describing the shape of the LDF i.e., all but f_0 , we exploit their correlation with d_{max} to parameterize

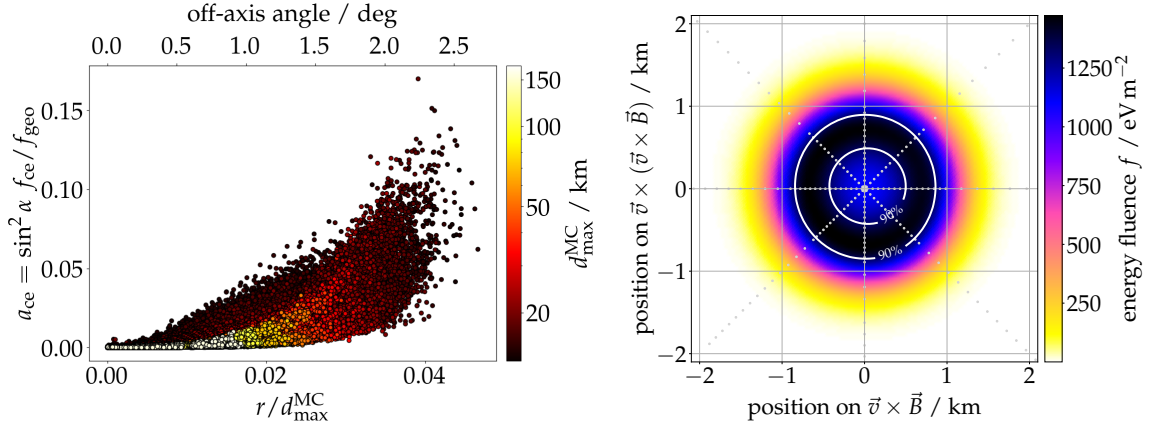


Figure 3: *Left:* Lateral distribution of the charge-excess fraction a_{ce} for all showers with zenith angles from 65° to 85° . Pulses affected by thinning and on the $\vec{v} \times \vec{B}$ axis are excluded. The lateral distance is shown in off-axis angles (the values in degree are annotated at the top). The color code shows d_{max} and highlights a dependency on the shower geometry. *Right:* Footprint of the geomagnetic emission estimated using a_{ce} of the example shower also shown in Figs. 1 and 2 (*left*). The footprint is fairly rotationally symmetric around a symmetry center which is slightly displaced w.r.t. the MC shower core at the coordinate origin.

them as a function of it. For details regarding the exact parameterizations see [7]. The scaling parameter f_0 can be replaced with the geomagnetic radiation energy E_{geo} with a clever normalization of Eq. (4).

The last step is to parameterize the interference between the dominant geomagnetic and sub-dominant charge-excess emission. For this purpose, we extract the charge-excess fraction $a_{ce} \equiv \sin^2 \alpha \cdot f_{ce}/f_{geo}$ from our simulations and investigate its correlation with air shower observables and observer positions. The geomagnetic angle α , the angle between the shower axis and Earth's magnetic field vector, already describes the scaling of the geomagnetic emission with the shower orientation to the magnetic field. With that one can derive the following expression for the geomagnetic emission which solely depends on a measurement of the emission in the $\vec{v} \times \vec{B}$ polarization

$$f_{geo} = \frac{f_{\vec{v} \times \vec{B}}}{\left(1 + \frac{\cos \phi}{|\sin \alpha|} \cdot \sqrt{a_{ce}}\right)^2}. \quad (5)$$

In Fig. 3 (*left*) the charge-excess fraction extracted from our simulations is shown as a function of the off-axis angle and d_{max} (color-coded). It can be seen that the fraction increases with the lateral distance from the shower axis but decreases with d_{max} . After several iterations of a parameterization for a_{ce} [21, 22], we arrived at the following expression which allows us to determine the geomagnetic emission with an accuracy of 2% for all zenith angles between 65° and 85°

$$a_{ce} = \left[0.348 - \frac{d_{max}}{850.9 \text{ km}}\right] \cdot \frac{r}{d_{max}} \cdot \exp\left(\frac{r}{622.3 \text{ m}}\right) \cdot \left[\left(\frac{\rho_{max}}{0.428 \text{ kg m}^{-3}}\right)^{3.32} - 0.0057\right] \quad (6)$$

with ρ_{max} the air density at the shower maximum. Note, that for a given arrival direction, observation height, and atmospheric model, ρ_{max} can be calculated from d_{max} and hence is not a new fit parameter. An example of the footprint of the geomagnetic emission determine using a_{ce} is shown in Fig. 3

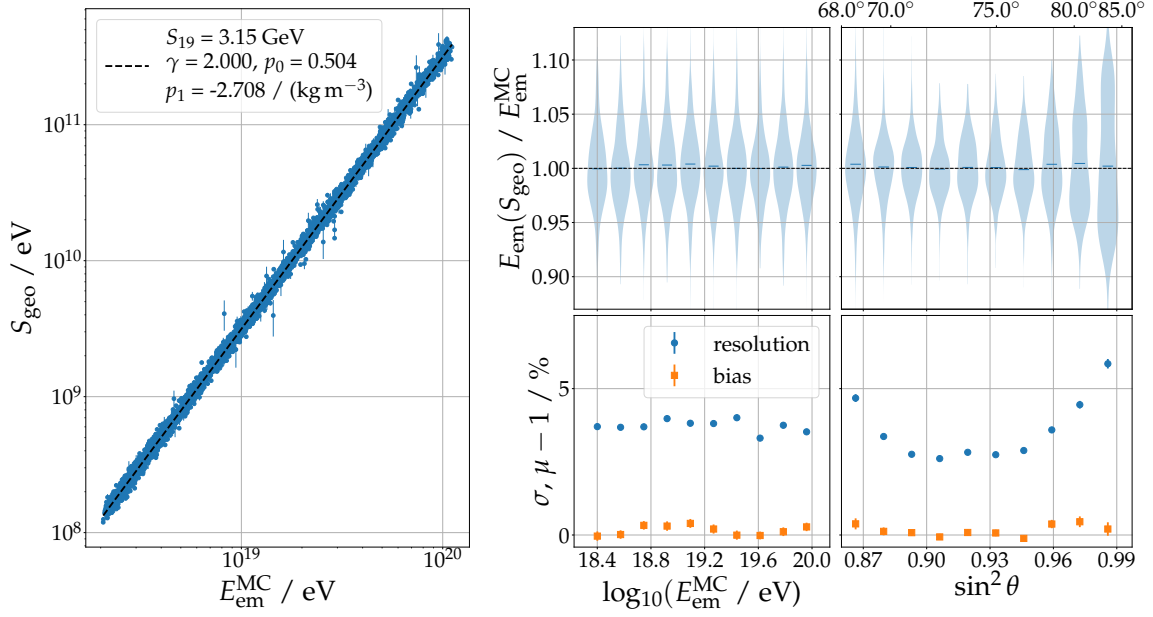


Figure 4: Reconstruction of the electromagnetic shower energy E_{em} for showers simulated for a 1.5 km-spaced antenna array. *Left:* Scatter plot of the radio-reconstructed electromagnetic shower energy as a function of the true electromagnetic shower energy. Legend indicates fit parameters according to Eqs. (7). *Middle & Right:* Bias and resolution of the reconstructed electromagnetic energy are shown as a function of the true energy (*middle*) and zenith angle (*right*). The full distributions are illustrated in the upper panels the profiles (mean and standard deviation) in the lower panels.

(*right*). The shown footprint is fairly rotationally symmetric which allows us to describe it with the 1-d LDF.

5. Energy reconstruction with a sparse antenna array

Now, we use the developed signal model to reconstruct the electromagnetic shower energy E_{em} using a set of simulations with the realistic detector layout. To reconstruct E_{em} from a fit to the radio-emission footprints which yield E_{geo} , we first describe the correlation of E_{geo} with the shower orientation to the magnetic field and air density at the shower maximum following the procedure from [23]. This ‘‘corrected geomagnetic radiation energy’’ S_{geo} can be correlated with E_{em} using a power law:

$$S_{\text{geo}} = \frac{E_{\text{geo}}}{\sin^2(\alpha)} \cdot \frac{1}{(1 - p_0 + p_0 \cdot \exp(p_1 \cdot [\rho_{\text{max}} - \langle \rho \rangle]))^2} \quad \text{and} \quad E_{\text{em}} = 10 \text{ EeV} \left(\frac{S_{\text{geo}}}{S_{19}} \right)^{1/\gamma}. \quad (7)$$

$\langle \rho \rangle = 0.3 \text{ g cm}^{-3}$ reflects a typical air density at the shower maximum of an inclined air shower with $\theta \sim 75^\circ$. In Fig. 4 (*left*) the correlation between S_{geo} and the true electromagnetic energy $E_{\text{em}}^{\text{MC}}$ is shown for all showers with at least 5 simulated antennas and a zenith angle above 68° . Additionally, we remove 16 out of 6210 showers due to their bad goodness of fit. The dashed line indicates the fitted power law, the legend shows the best-fit parameters of Eqs. (7). The accuracy of the reconstruction can be inspected in the same figure on the other panels which show the reconstructed

over the true electromagnetic energy. A resolution better than 5% for most of the phase space and no significant bias is found (cf. Fig. 4). We do not observe a significant dependency of those results on the primary cosmic-ray mass.

The presented results were obtained with the showers generated with the high-energy hadronic interaction model QGSJETII-04. We repeated the reconstruction using Sibyll2.3d generated showers and found no significant change in the reconstruction accuracy and only a 2% shift in the absolute scale of S_{19} (while the other parameters were kept fixed).

6. Conclusion

We presented a signal model for the reconstruction of very inclined air showers with zenith angles between 65° and 85° . With only two fit parameters, the geomagnetic radiation energy E_{geo} and the distance between the shower maximum and the ground d_{max} (+ two core coordinates), the model is very well suited for the reconstruction of showers detected with kilometer-sparse antenna arrays. For the particular case of an array with a spacing of 1.5 km and 5 or more antenna signals, we obtained an energy resolution better than 5%. Those results can be considered the “intrinsic” accuracy of the model as many effects present in real observations (noise, uncertain shower axis, etc.) are unaccounted for. However, the signal model has been used in a more realistic study with promising results, see chapters 8 and 9 in [24].

The signal model takes into account the orientation of the showers to the Earth’s magnetic field as well as the atmospheric density profile. Hence, it can be adapted to do different magnetic field orientations and atmospheric conditions. The scaling of the emission strength with the magnetic field strength was found to be $E_{\text{geo}} \sim |\vec{B}|^{1.8}$ [23] and has to be considered when adapting this model. Utilizing the lateral distance in the parameterization of a_{ce} invokes a minor dependency on the observation height. More crucial, the parameterization of the LDF for the geomagnetic emission and potentially the charge-excess fraction will depend on the utilized frequency band and need to be renewed for other frequency bands.

References

- [1] PIERRE AUGER, *Phys. Rev. D* **91** (2015) 032003 [1408.1421].
- [2] PIERRE AUGER, *Phys. Rev. Lett.* **117** (2016) 192001 [1610.08509].
- [3] E.M. Holt et al., *Eur. Phys. J. C* **79** (2019) 371 [1905.01409].
- [4] PIERRE AUGER, *Phys. Rev. Lett.* **126** (2021) 152002 [2102.07797].
- [5] PIERRE AUGER, *JCAP* **1810** (2018) 026.
- [6] PIERRE AUGER, *PoS ICRC2019* (2021) 274.
- [7] F. Schlüter and T. Huege, *JCAP* **2023** (2023) 008 [2203.04364].
- [8] S. Ostapchenko, *Phys. Rev. D* **83** (2011) 014018 [1010.1869].
- [9] E.-J. Ahn et al., *Phys. Rev. D* **80** (2009) 094003 [0906.4113].
- [10] F. Riehn et al., *Phys. Rev. D* **102** (2020) 063002 [1912.03300].
- [11] M. Bleicher et al., *J. Phys. G* **25** (1999) 1859 [hep-ph/9909407].
- [12] D. Heck et al., *FZKA Report 6019*, Forschungszentrum Karlsruhe (1998).
- [13] T. Huege, M. Ludwig and C.W. James, *AIP Conf. Proc.* **1535** (2013) 128.
- [14] K. Werner and O. Scholten, *Astropart. Phys.* **29** (2008) 393 [0712.2517].
- [15] K.D. de Vries et al., *Astropart. Phys.* **34** (2010) 267 [1008.3308].
- [16] T. Huege, *Phys. Rept.* **620** (2016) 1.
- [17] K.D. de Vries et al., *Phys. Rev. Lett.* **107** (2011) 061101 [1107.0665].
- [18] S. Chiche et al., *PoS ICRC2021* (2021) 194 [2202.05886].
- [19] F. Schlüter et al., *The European Physical Journal C* **80** (2020) 643.
- [20] C. Glaser et al., *Astropart. Phys.* **104** (2019) 64.
- [21] T. Huege et al., *EPJ Web Conf.* **216** (2019) 03009 [1808.00729].
- [22] T. Huege, F. Schlüter and L. Brenk, *PoS ICRC2019* (2021) 294 [1908.07840].
- [23] C. Glaser et al., *JCAP* **1609** (2016) 024.
- [24] F. Schlüter, Ph.D. thesis, KIT, Karlsruhe, IAP, 2022. 10.5445/IR/1000149113.